This deliverable has been quality checked and approved by CityHush Coordinator
Nils-Åke Nilsson

TABLE OF CONTENTS

0 EXECUTIVE SUMMARY

0.1 OBJECTIVE OF THE DELIVERABLE

To develop low noise tyre concept designs for low noise roads (smooth surfaces).

0.2 DESCRIPTION OF THE WORK PERFORMED SINCE THE BEGINNING OF THE PROJECT

We have obtained new results on the vibrations of rolling tyres, aimed at noise prediction for tyres of given design on a smooth road surface. This new approach incorporates existing models, developed within the UCAM group, of smooth road-tyre interaction and belt vibration, but includes additional features that are required for real tyre patterns. To this end, our model allows variable tread block size and grooves along the belt circumference; the density and angle of these grooves may also vary laterally. The key innovation is to treat the tyre belt as a laterally stacked series of rings, each of which is equipped with a set of viscoelastic springs around its circumference. We have used this construction to mimic the details of actual tyre patterns and, in conjunction with existing belt and road-contact models, predict belt vibrations.

0.3 MAIN RESULTS ACHIEVED SO FAR

This construction has been applied to develop a ring discretisation for a real tyre that shows strong lateral variations. We find that the vibration amplitude is concentrated on a set of parallel lines in frequency-wavenumber space and that the tread pattern dictates the occurrence and spacing of these lines. The tyre belt vibrations in the axle frame of reference are shown to be a superposition of small amplitude periodic fluctuations and the temporal mean displacement over a rotation. The computed belt shape is consistent with that inferred from laboratory experiments.

0.4 EXPECTED FINAL RESULTS

The vibration calculation will be linked to radiated noise via the Boundary Element Method. Noise predictions for practical tread patterns will be made.

0.5 POTENTIAL IMPACT AND USE

Linkage to a Boundary Element calculation will deliver a powerful tyre/road noise prediction tool. This will enable quantification of the influence of real tyre tread parameters on radiated noise, and contribute towards the development of novel tyre designs for optimal noise characteristics. Such designs will lead to reduced vehicle noise pollution.

0.6 PARTNERS INVOLVED AND THEIR CONTRIBUTION

Goodyear has provided maps of representative tread patterns.

0.7 CONCLUSIONS

The approach has been tested with a particular tyre that shows strong lateral and circumferential variations. The predictions of the model remain robust and clear; namely that the tread pattern dictates the occurrence and spacing of the parallel lines in frequency-wavenumber space on which the vibration amplitude is concentrated. Furthermore, the tyre belt vibrations in the axle frame of reference are a superposition of small amplitude periodic fluctuations and a (temporal) mean displacement. We now have an integrated model that incorporates an empirical smooth road contact model, a full treatment of belt vibrations including sidewall effects and a realistic representation of tyre tread patterns. The next step is to couple this model to a Boundary Element Method and deliver a predictive tool for acoustic radiation fields from a rolling tyre.

ABSTRACT

This report extends our previous work on the vibrations of rolling tyres aimed at noise prediction for tyres of given design. The main thread in this work is to address various limitations that restricted the application of the prior model to real tyre patterns. To this end, we develop an enhanced model that allows variable tread block size as well as grooves along the belt circumference; the density and angle of these grooves may also vary laterally. The key innovation is to treat the tyre belt as a laterally stacked series of rings, each of which is equipped with a set of viscoelastic springs around its circumference. It is shown how to use this construction to mimic the details of actual tyre patterns and, in conjunction with existing belt and road-contact models, predict belt vibrations.

This general construction is applied to develop a 17-ring discretisation for a particular (Goodyear XP4609) tyre that shows strong lateral variations. It is shown that the vibration amplitude is highly concentrated on a set of parallel lines in frequency-wavenumber space and that the tread pattern dictates the occurrence and spacing of these lines. In general, the tyre belt vibrations in the axle frame of reference are found to be a superposition of small amplitude periodic fluctuations and the temporal mean displacement over a rotation. The computed belt shape is also shown to be consistent with that inferred from laboratory experiments.

1. INTRODUCTION

This report presents new results on the development of quiet tyre designs for quiet road surfaces, an objective that is addressed under the auspices of the CityHush project (http://www.cityhush.org/). Our previous report on this topic [2] described what was termed an integrated model of the vibrations of a rolling tyre on a (smooth) road surface. That model, written in MATLAB, computes the tyre belt vibration field due to the forces resulting from the sequence of impacting tread blocks as the tyre rolls forward. The computations are done in the frequency-wave number domain, as this allows direct coupling of existing models of smooth road-tyre interaction and belt vibration and also offers various advantages in respect of immediate physical interpretation of the results. The model used adaptations of prior work on tread block contact with a smooth road [3] and on belt vibrations due to an impulsive point source [1], which is why it was termed an integrated model. This approach produces interesting results that are perfectly consistent with the new results given here; however, there are also several limitations. Indeed the integrated model, does not quite meet the demands imposed by the complex nature of real tyre designs.

The new work presented here is aimed at bridging the gap between our previous model and what is needed to have a useful predictive model of tyre noise including the role of design parameters. The main additional functionality required is the capacity to incorporate variations in tread block size along the belt circumference as well as lateral variations in groove density and angle. It is not obvious how to achieve this within our previous approach; we are therefore led to develop an alternative, related model that fits our purpose. Section 2 gives a brief overview of how the previous model worked and of its limitations and then introduces the ring discretisation. The key innovation is to treat the tyre belt as a laterally stacked series of rings, each of which is equipped with a set of viscoelastic springs around its circumference. It is then

possible to model the appearance of a groove along the circumference by a node that does not have an attached spring; the lateral variation arises from staggering the 'no spring' nodes relative to one another in the ring sequence to reflect the effect of the acute groove angle. The overall belt displacement may be taken as the lateral average across the rings.

This general construction is applied to develop a 17-ring discretisation for a particular (Goodyear XP4609) tyre that shows strong lateral variations. It is shown that the vibration amplitude is highly concentrated on a set of parallel lines in frequency-wavenumber space and that the tread pattern dictates the occurrence and spacing of these lines. In general, the tyre belt vibrations in the axle frame of reference are found to be a superposition of small amplitude periodic fluctuations and the temporal mean displacement over a rotation. The computed belt shape is
also shown to be consistent with that inferred from laboratory experiments.

The ring discretisation retains the assumed shape for the undeformed belt that was originally derived from experiments [3] but we transform the Fourier displacement components into a fixed (axle) frame of reference and thus check the consistency of the assumption. It should be noted that the modular nature of the numerical model facilitates computations with an arbitrarily chosen tyre. Furthermore, the 17-ring discretisation used here is very much at the upper end of what is required in practice; although the number of rings is not an issue in principle, the construction of the full belt response is awkward for such a large number.

2 THE RING DISCRETISATION: MOTIVATION AND DEVELOPMENT

The aim of our first tyre vibration model [2] was to compute the belt vibrations due to road contact of successive tread blocks as the tyre undergoes a single full rotation. The algorithm starts from a given tread block geometry, adds the option of a gap between successive blocks and produces a resultant force on the belt as a function of time t and circumferential position θ. The overall force on the belt is then assembled from the individual block forces; this requires some care as several blocks may simultaneously be in partial contact with the road surface. The response to this more general forcing is then derived from the impulse response via convolution. The main problem with this model is that the approach to assembling the forcing on the belt is difficult to apply to a realistic tyre pattern. There is no difficulty when, as in [2], one has a given number of tread blocks with or without a fixed gap between successive blocks. Lateral variation within a block may be accommodated by varying nodal spring stiffness values but irregular block sizes, or indeed a variable gap size, would clearly cause problems. The enhanced model allows variable tread block size as well as grooves along the belt circumference; the density and angle of these grooves also vary laterally.

However, an examination of the real tyre image shown in Figure 1 shows that circumferential variations in block size and lateral variations in groove angle cannot be ignored. An alternative formulation is to regard the tyre belt as a laterally stacked series of rings, each of which is equipped with a set of nodes around its circumference. Ring models have been used before [5], [4] to study tyre deformations, mainly as simple analytical models for purposes of comparison with results from a discretised method. In our case, the ring discretisation lies within a full numerical approach. A groove or gap between blocks is modelled by a node that does not have an attached spring; Figure 2 shows the single ring construction in schematic form. It is then easy to build a sequence

of such rings with the 'no spring' nodes staggered relative to one another as this reflects the effect of the acute groove angle that can be seen in Figure 1. At each node, where there is a spring present, the applied force is typically that measured by F. Liu in his experiments on loaded tyres [3] although we also test the influence of the force parameters by comparison with a synthetic forcing function as in our previous report [2]. It is then possible to model the appearance of a groove along the circumference by a node that does not have an attached spring; the lateral variation arises from staggering the 'no spring' nodes relative to one another in the ring sequence to reflect the effect of the acute groove angle. The current model remains as close as possible to the original vibration model. It uses the same belt vibration model and the same empirical force and viscoelastic constitutive law displacement at each spring.

Once a basic pattern has been identified, it is implemented in the block pattern module that generates the nodal data. The relevant forces are then assembled using the nodal and contact force input; for each ring, the resultant forcing is convolved with the response of that ring to give the displacement component.
Note that although the individual rings are not directly coupled, in the sense that the spring displacement at each node is determined purely by the forcing at that node, the total belt response on any ring, at a given angular order *n* and frequency ω, is obtained by summing over the full set of lateral input points. The overall assembly of a full vibration model for a given tyre should follow the sequence below:

1. Identify the basic pattern along the circumference.
2. Inspection of the lateral variation suggests minimum number of required rings, *R*.
3. Edit the block pattern code which outputs a nodal spring data file and thus generates the applied force on each ring, $F_k = F_k(n,\omega) k = 1,...R$
4. Calculate the response of each ring in frequency-wavenumber space from the belt model via

$$g_k(n,\omega) = \sum_{j=1}^{R} G_{kj}(n,\omega) \qquad (1)$$

where G_{kj} denotes the belt response at $l = l_k$ due to a unit impulse at $l = l_j$.

5. Use the convolution theorem to deduce the displacement at each ring

$$\hat{v}(n,\omega) = F_k(n,\omega) g_k(n,\omega)$$

with the resultant belt displacement identified as

$$\hat{v}(n,\omega) = \frac{1}{R} \sum_{k=1}^{R} \hat{v}_k(n,\omega)$$

3 MODEL RESULTS

It is convenient to itemise the procedure that has been adopted to generate the input required for tyre vibration model. This procedure is informal and assumes access to an

image of a tyre belt section such as that shown in Figure 1; however, the image is only used here in a qualitative way. The ring discretisation is then developed as follows:

1. Use the tyre image to generate a ring discretisation for the full tyre. Figure 1 suggests firstly that the 180 mm belt width divides naturally into five zones, with parallel grooves at a fixed angle within each zone. The central zone is distinguished by the absence of any grooves, which implies that a single ring should be sufficient to represent it.

2. The idea with the other zones is an accurate representation that uses the minimum number of rings. The required number is dictated by the severity of the groove angle; thus by inspection it seems reasonable to use 3 rings to represent zone 1 (reading from the bottom up i.e. between 0 and 40 mm) and 5 rings for zone 2. The full ring discretisation consists of 17 rings, following the sequence 35153 across the five zones within the belt.

3. In order to account for the effect of the groove angle, the arrangement of springs along each ring is staggered, by one node in this example, relative to its nearest neighbours.

4. Figure 1 also suggests that the tread block size varies along the belt circumference. A reasonable circumferential pattern prompted by the image is to split the blocks into three lengths, small medium and large, and then repeat the basic sequence S M L M. An illustration of the scheme is given in Figure 2.

It is also important to ensure that the model satisfies the constraint that each ring has the same number of 'no-spring' nodes, although the circumferential location of these nodes varies laterally due to staggering between adjacent rings. This requirement implies a constraint on the number of nodes in the basic pattern, namely a certain minimum number of such nodes is required in order to accommodate the lateral variation in the pattern. For this reason, 32 nodes are used here. Initially the algorithms were tested with a 5-zone model rather than the full 17-ring discretisation, because computing with the full model required some engineering to avoid memory problems. However, all of the results shown were obtained with the full model.

4. FRAME TRANSFORMATION

It has been tacitly assumed, thus far, that all quantities are computed in the belt frame of reference since the belt vibration model naturally uses this frame. However, since our motivation lies in modelling the noise produced by rolling tyres, we must switch to a frame in which the belt rotates. To this end we introduce the axle frame of reference; if ϕ denotes the angle of a point on the tyre circumference in the axle frame and θ denotes the corresponding angle in the rotating belt frame as shown in figure 3, then the angles are related by

$$\phi = \theta - \Omega t \qquad (2)$$

Figure 3 should clarify the sign conventions used; the tyre rotates in the direction shown, opposite to that of increasing ϕ and θ, so that the angles of tread blocks in the contact

patch increase with time. Note that within the terms of the ring discretisation it is perfectly admissable to restrict attention to 1D geometry where the displacement components depend only on time t and circumferential angle θ. Dependence on *l* i.e. variation across the belt is included by varying the ring index. A generic displacement component w may then be written in the belt frame of reference as

$$w(\theta,t)=\sum_{\substack{m=0\\ n=-N}}^{M,N} w_{mn}\exp(im\Omega t)\exp(in\theta) \tag{3}$$

Let $v(\phi,t)$ denote the same component in the axle frame; equation (2) makes it evident that v is given by

$$v(\phi,t)=\sum_{m,n} w_{mn}\exp(i(m+n)\Omega t)\exp(in\phi) \tag{4}$$

The form of this expression suggests that it may be rewritten in a form analogous to the form of equation (3) by changing the frequency mode number via $m'=m+n$, so that

$$\begin{aligned} v(\phi,t) &= \sum_{m',n} w_{(m'-n)n}\exp(im'\Omega t)\exp(in\theta) \\ &= \sum_{\substack{n=-N\\ m\geq n}}^{N,M+n} w_{(m-n)n}\exp(im\Omega t)\exp(in\phi) \end{aligned} \tag{5}$$

5 RESULTS AND DISCUSSION

Figure 4 shows the logarithmic radial velocity in the belt frame computed for a representative single ring; there are 256 spatial nodes along the circumference in this and all of the results shown. It is clear that the vibration amplitude achieves its maximum values along the primary line $m+n=0$; the figure also shows the blurring effect that occurs when the total number of nodes is not exactly divisible by the number in the basic pattern. Note also that the spacing between the parallel lines where the significant amplitudes are concentrated is dictated by the number of pattern repetitions within the circumference, 8 in this case. The simplest case is the special case of the central ring 9 which is the only ring with a spring present at each node. Therefore, the force in the contact patch is time-invariant and the vibrations are confined to the primary line as shown in figure 5. Figure 6 gives the generic ring displacement in (n,ω) space but viewed from the fixed (axle) frame of reference.

Figure 7 shows the predicted displacement after Fourier inversion, in both the axle and belt frames for this ring. It is clear that the axle frame displacement does not vary with time, but instead has the fixed angular dependence that is shown in figure 8 and resembles the shape of a squashed cardioid. It is obvious that the corresponding shape in the belt frame, deduced from the results shown in figure 7, should be just the fixed shape rotated at a rate Ω and that is what is obtained and illustrated in figure 9.

The obvious question is then the corresponding results for other rings with time-dependent contact forces. Figure 10 shows the maximum and minimum displacements in each ring; in both cases, the results are symmetric and peak about the central ring. Analogous results are shown for a generic ring, for definiteness ring 13 is actually used; the calculated displacement in both frames as shown in figure 11. The first point of note is that the result in the axle frame $v(t,\phi)$ in contrast to that shown in figure 7, varies with time in a periodic fashion, with period $p = T/8$, which reflects the fact that the tyre belt model has exactly eight repetitions of the same basic pattern. However, figure 12 clearly illustrates the small amplitude of the time dependence.

It is clear that the results are compatible with the analytical form

$$v(t,\phi) = \langle v \rangle(\phi) + \varepsilon\, f(\Omega t) \tag{6}$$

where ε is a small (compared with 1) positive parameter which may vary with ϕ and the fluctuation function *f* is periodic with period $\pi/4$. The angular brackets denote, as usual, an average over a single rotation. The accuracy of this approximation is demonstrated in figure 12 when the numerical result is compared with the simple analytical approximation given by equation (7) at different times.

$$v(t,\phi) = \langle v \rangle(\phi) + .001\cos(\Omega t - \frac{5\pi}{4}) \tag{7}$$

Note that the amplitude and phase of the fluctuations function in the last expression were found by inspection and are particular to this example. The important point is that the perturbation of the belt shape is accurately approximated by the superposition of the mean displacement over a rotation with a periodic small amplitude fluctuation. Furthermore, the belt frame displacement ought to be close to rotations of the mean shape in the axle frame, which, as figures 13 and 14 confirm, it is. Figure 15 shows the mean belt shape for completeness. All of these conclusions are shown for a particular ring but have also been tested successfully for the others.

Finally, the shape of the rolling tyre belt is obtained by lateral averaging and superimposing the initial circular shape. This shape is shown in figure 16 and it is consistent with that obtained from experiment in Liu's thesis and used in the road contact model and in the nodal ring discretisation presented here.

6 CONCLUSIONS

The new model presented here builds directly on our previous modelling work on rolling tyre vibrations and uses many of the same components. The novel aspect is the introduction of a ring discretisation to allow the application of the modelling to real tyre patterns. The enhanced model admits variable tread block size as well as grooves along the belt circumference with lateral variation in the density and angle of these grooves.

The approach is applied to a particular (Goodyear XP4609) tyre that shows strong lateral variations, and therefore requires an unusually high number of rings for an accurate representation. It is shown that the vibration amplitude is highly concentrated

on a set of parallel lines in frequency-wavenumber space and that the tread pattern dictates the occurrence and spacing of these lines. In general, the tyre belt vibrations in the axle frame of reference are found to be a superposition of small amplitude periodic fluctuations and the temporal mean displacement over a rotation. The computed belt shape is also shown to be consistent with that inferred from laboratory experiments and used in the component road contact model. The next step in the overall program is to couple this model to a boundary element method and deduce tyre acoustic radiation fields.

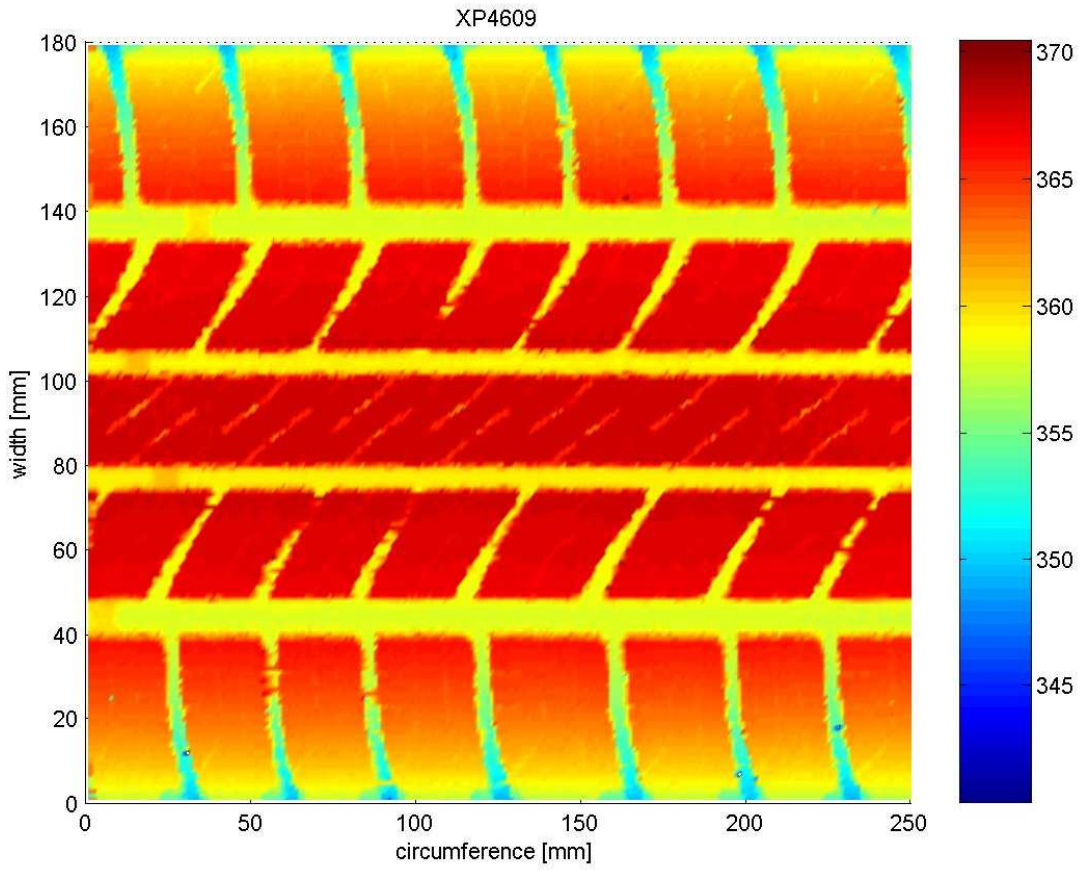

Figure 1: Image of belt section showing 2D variation in block size and groove patterns; the tyre is Goodyear XP4609

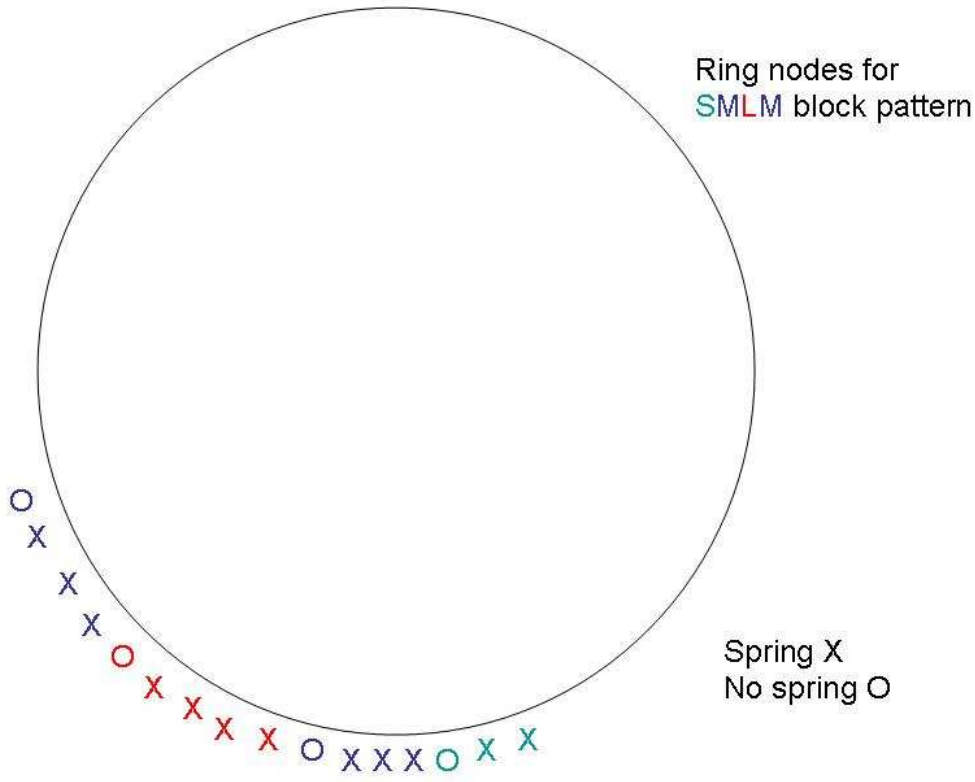

Figure 2: Schematic of nodal ring pattern showing short medium long medium sequence; for clarity the blocks are shown with 3, 4 and 5 nodes respectively. The simulation results were obtained with a basic pattern of 32 nodes reflecting the block nodal sequence 6 8 10 8.

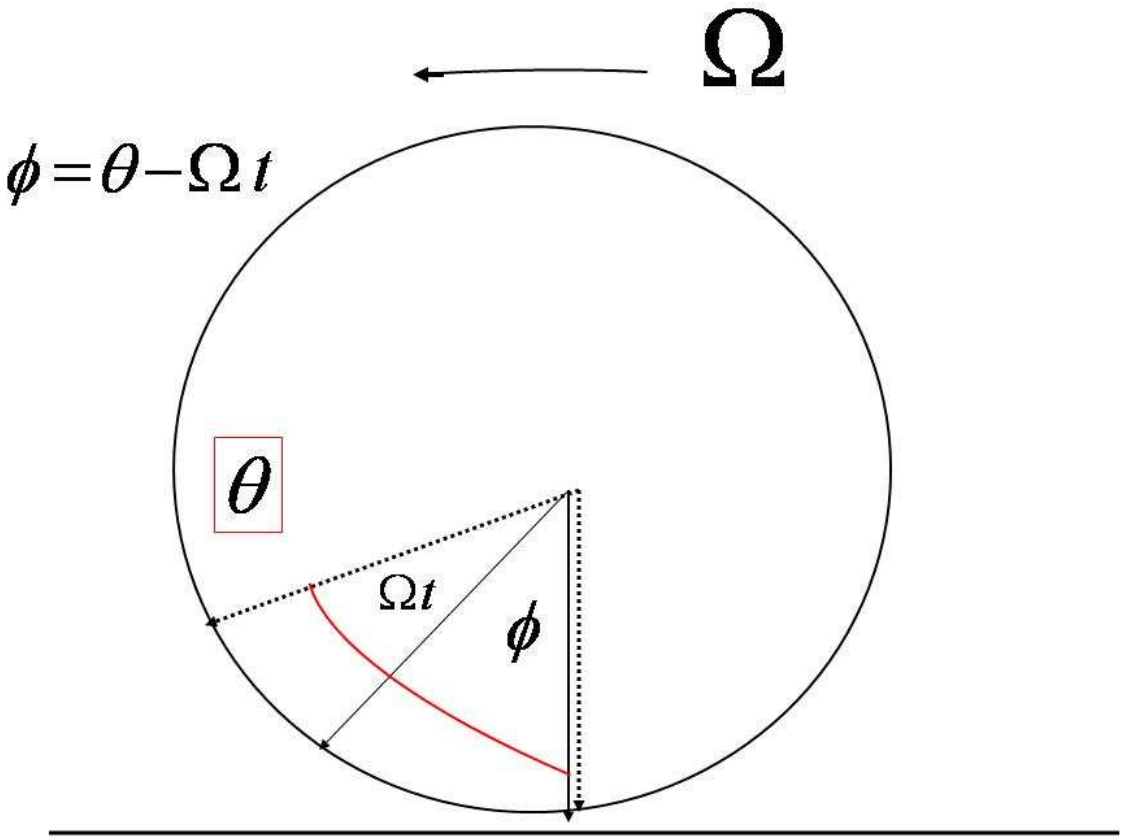

Figure 3: Definition of the angles ϕ and θ used to measure circumferential position in the axle and belt frames respectively. Note that both angles increase in the direction opposite to that of the tyre rotation.

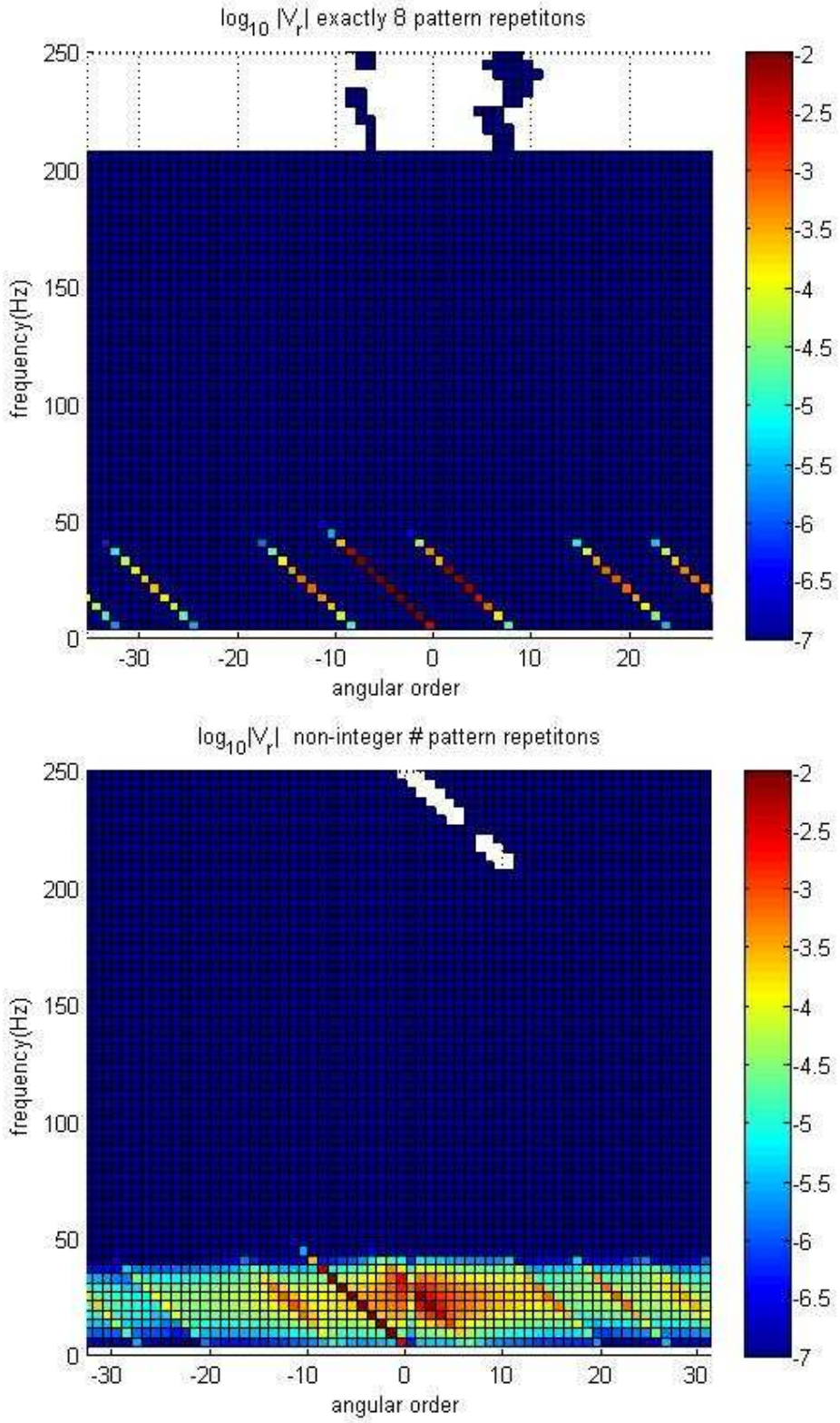

Figure 4: Vibration results for generic ring where (a) total node number is an integer multiple of node number in repeated tread block pattern SMLM and (b) model input is more accurate block pattern SSMLM which does not give an integer node number ratio.

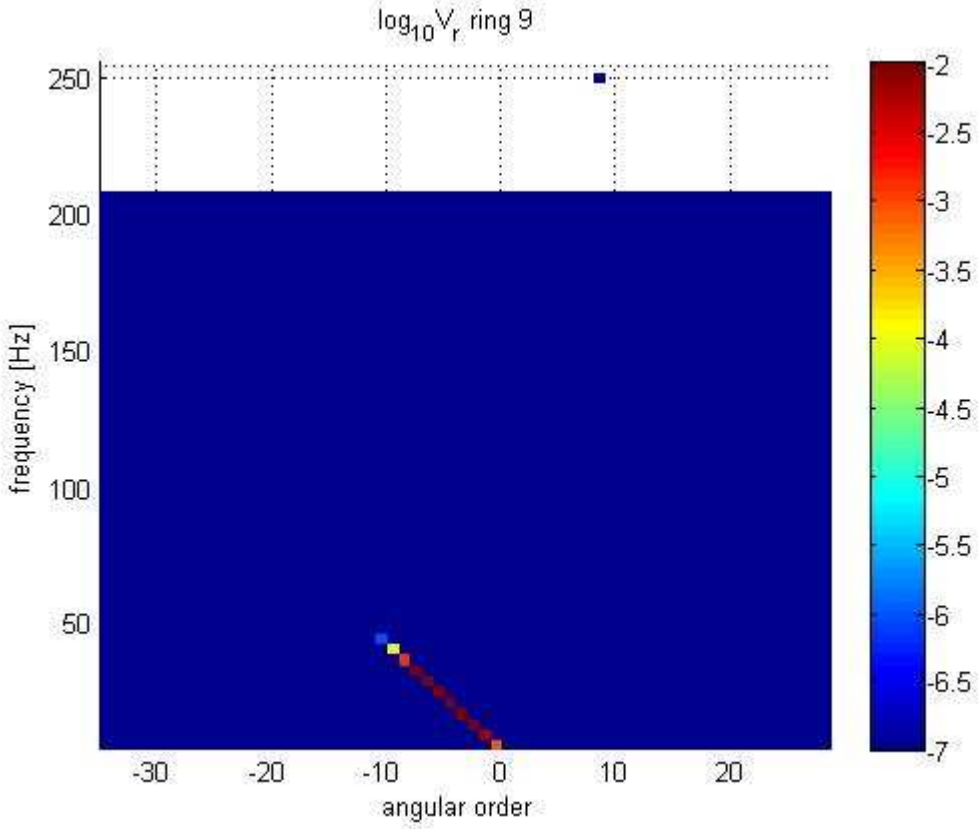

Figure 5: Vibration results for central ring in 17-ring discretisation. The velocity is wholly confined to the primary line $m + n = 0$ because the absence of any groove means that the applied force is constant over a rotation for any block pattern.

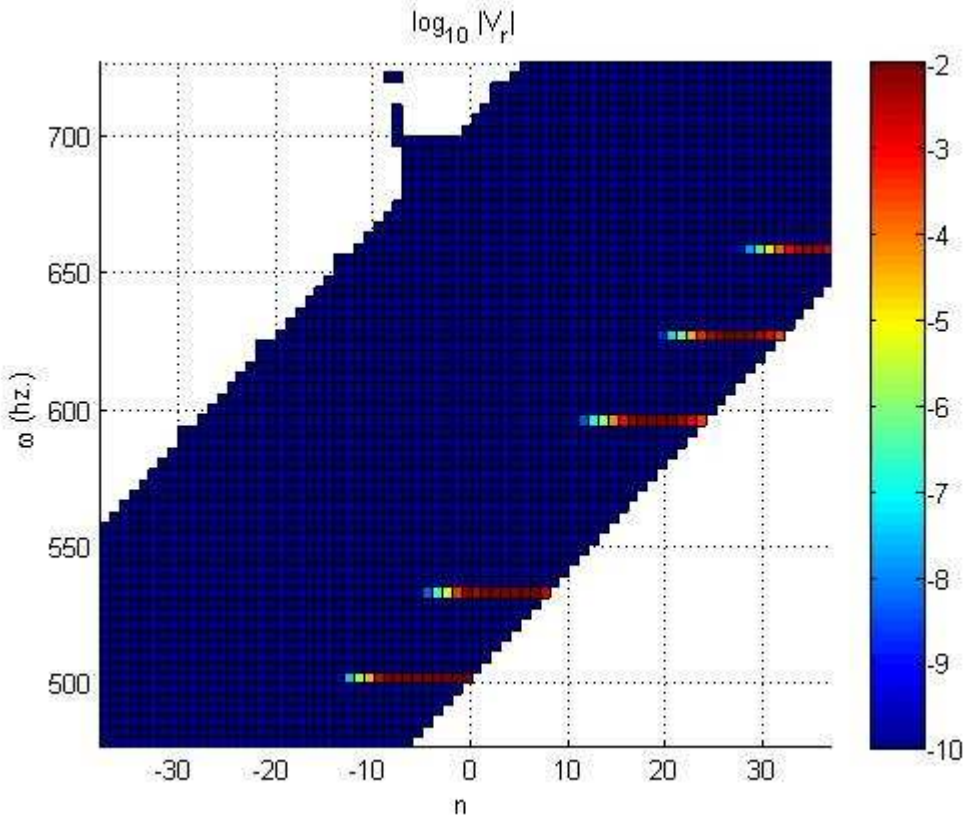

Figure 6 Log displacement for generic ring in the axle frame

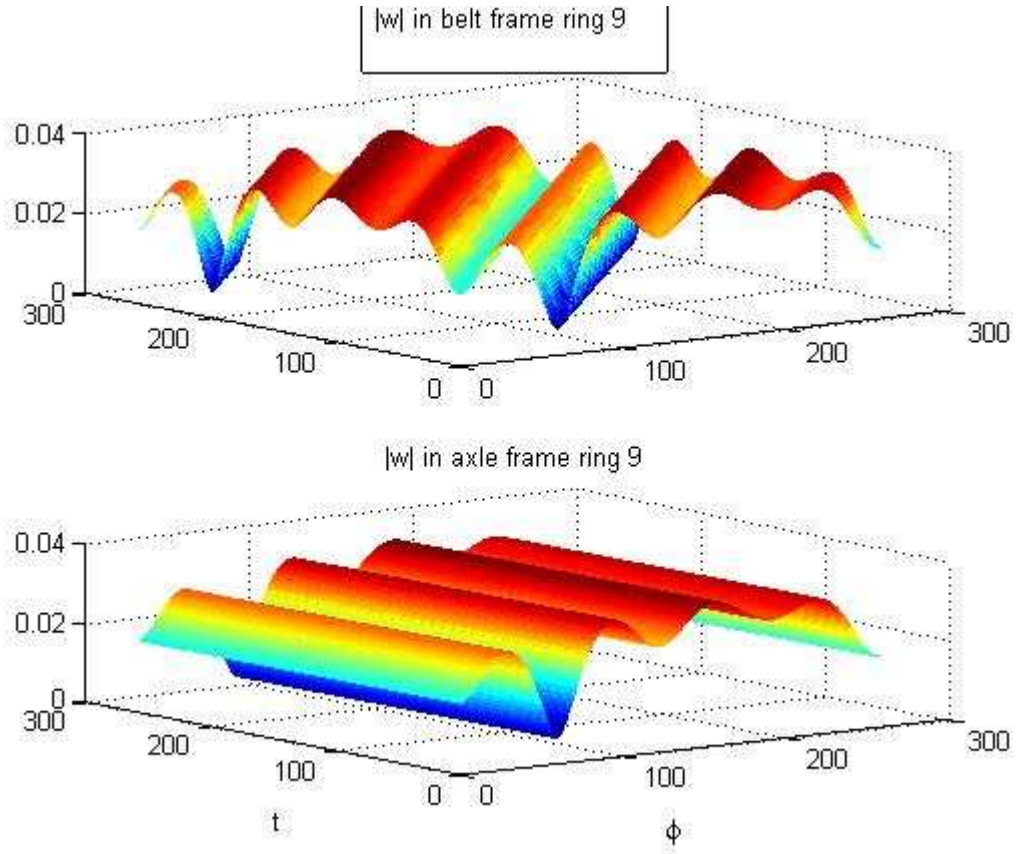

Figure 7: The central ring 9 displacement in the belt and axle frames.

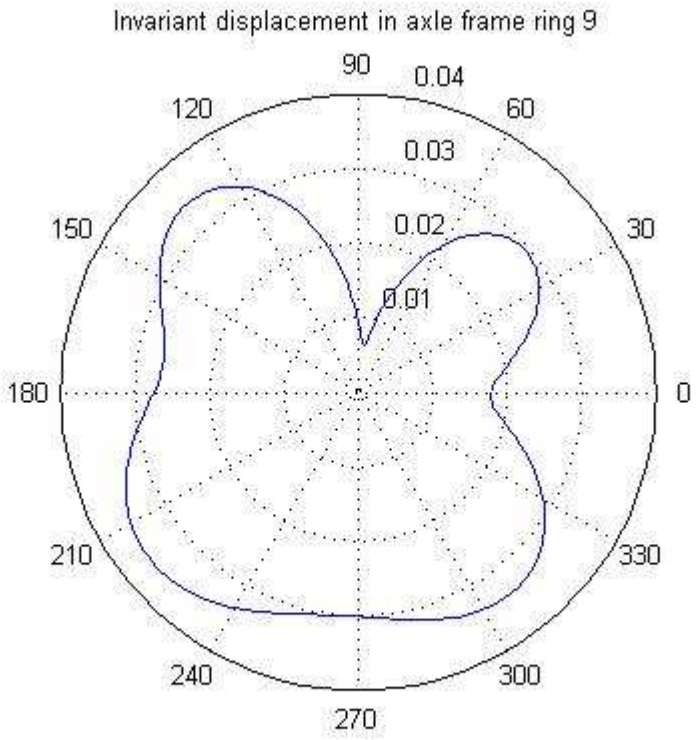

Figure 8: Polar plot of ring 9 displacement in the axle frame

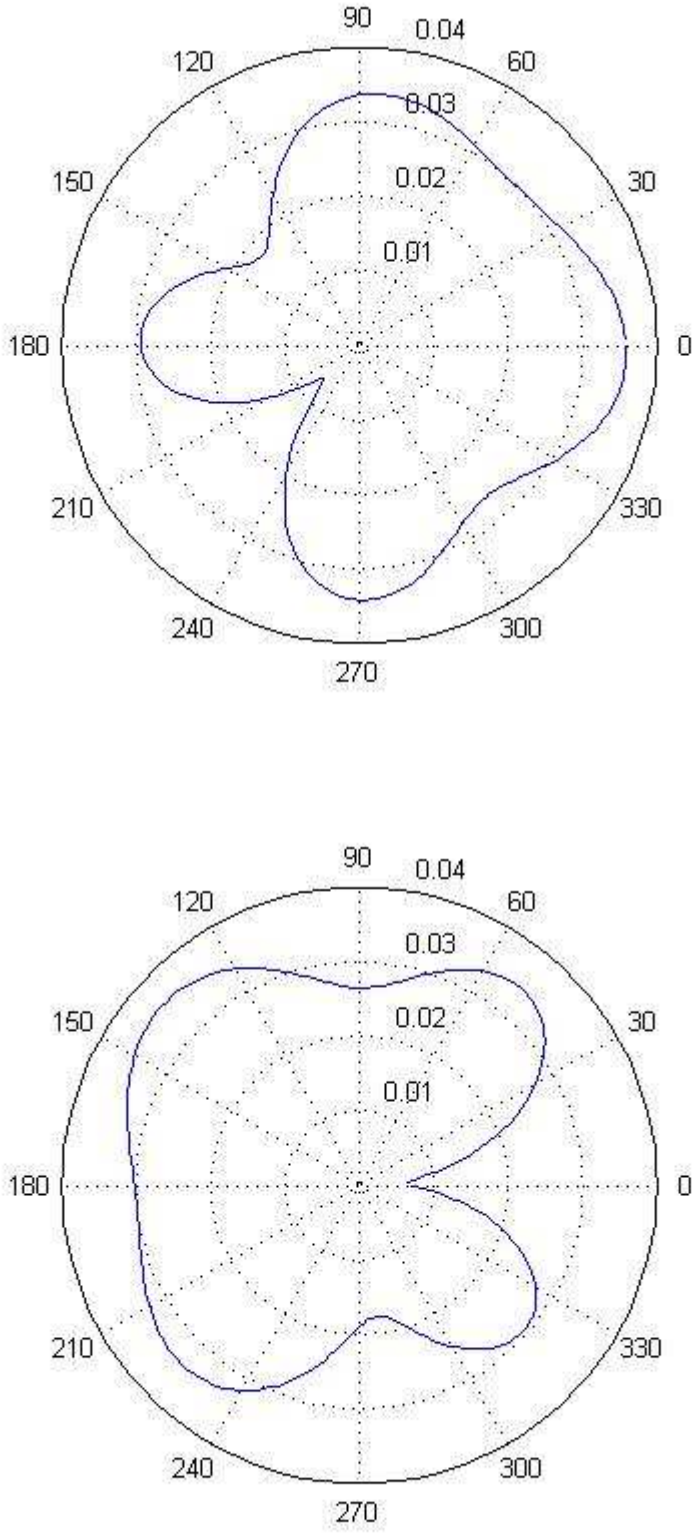

Figure 9: Polar plot of ring 9 displacement in the belt frame at 2 different times (.08 and .16 sec respectively); results are clearly rotations of the shape given in the previous figure.

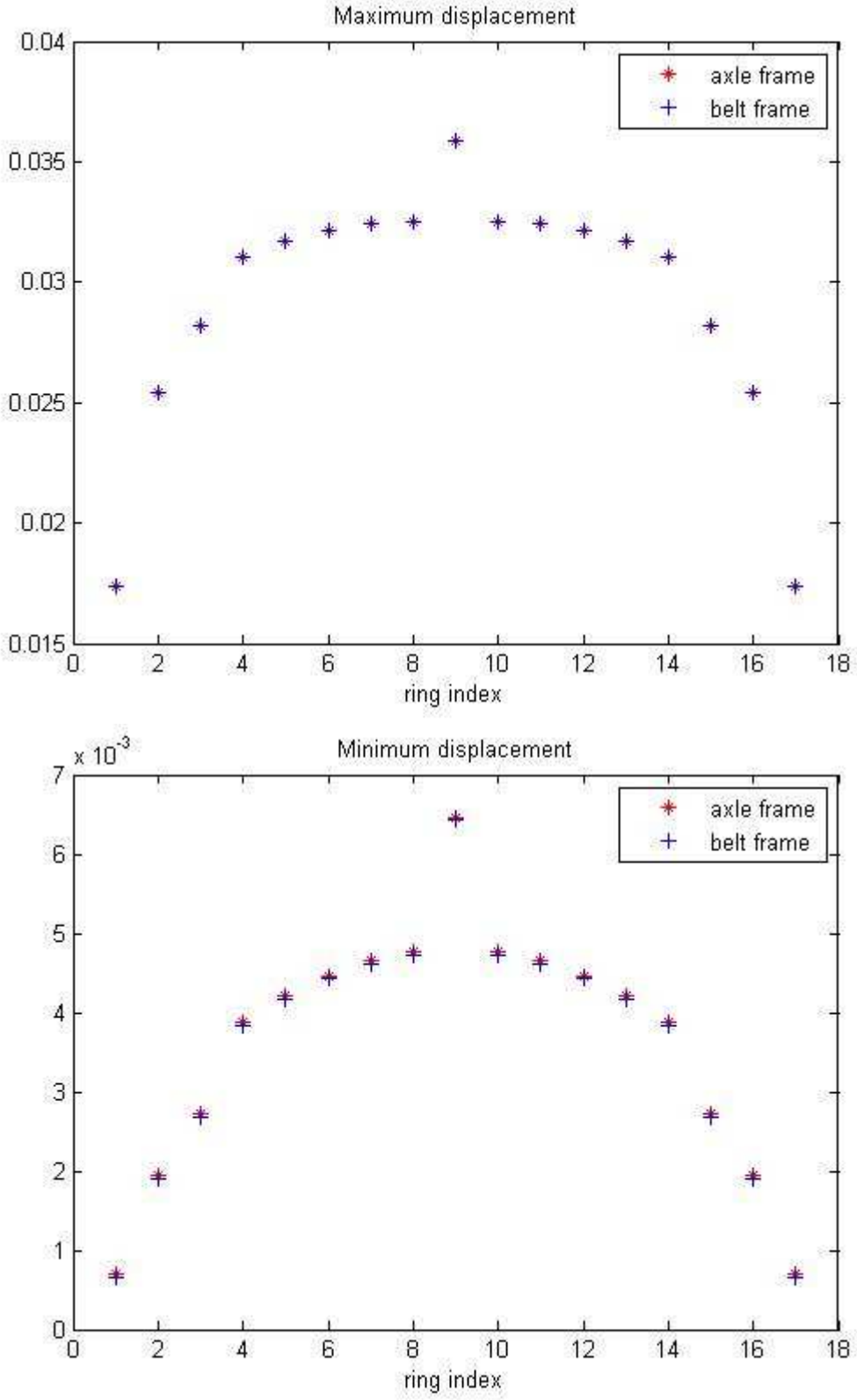

Figure 10: Maximum and minimum displacements in each ring; in both cases, the results are symmetric about the central ring.

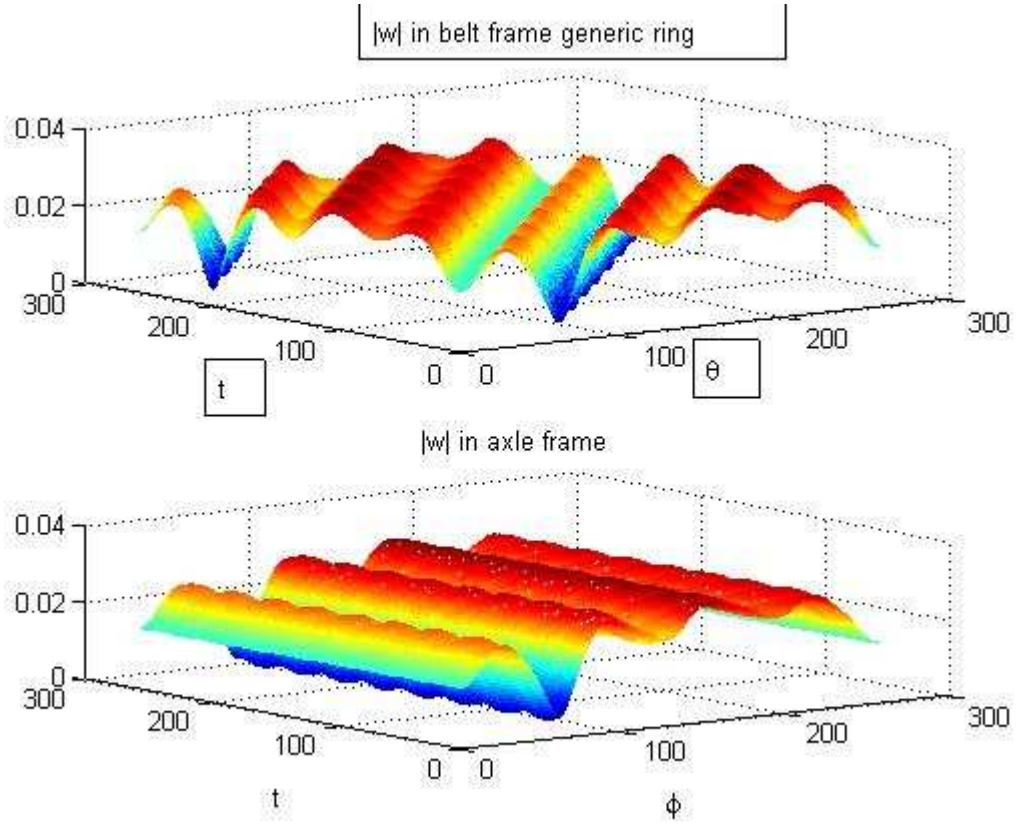

Figure 11: Generic ring displacement in the belt and axle frames.

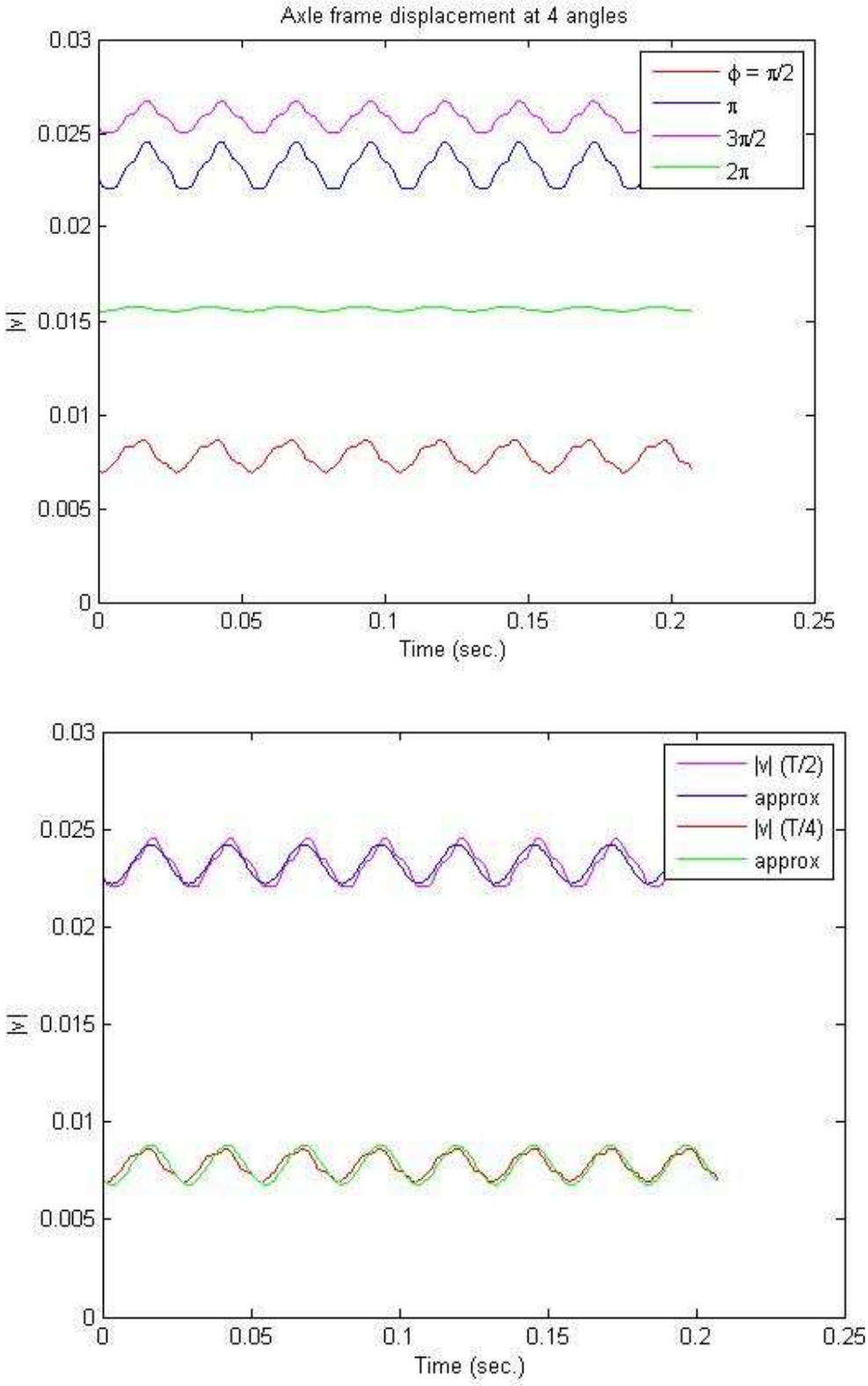

Figure 12: Generic ring displacement in axle frame as a function of time at 4 angles (top). The bottom figure illustrates the accuracy of simple analytical approximation, i.e. periodic small amplitude fluctuations about the temporal mean, to axle frame displacements.

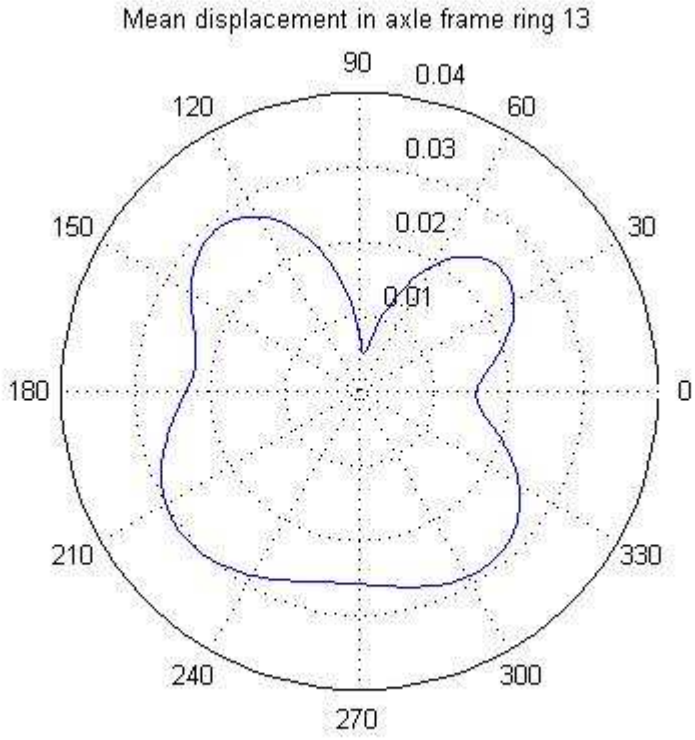

Figure 13: Polar plot of ring 13 mean displacement in the axle frame. The shape is similar to invariant displacement of the central ring, but with lower amplitude at a ratio of .85.

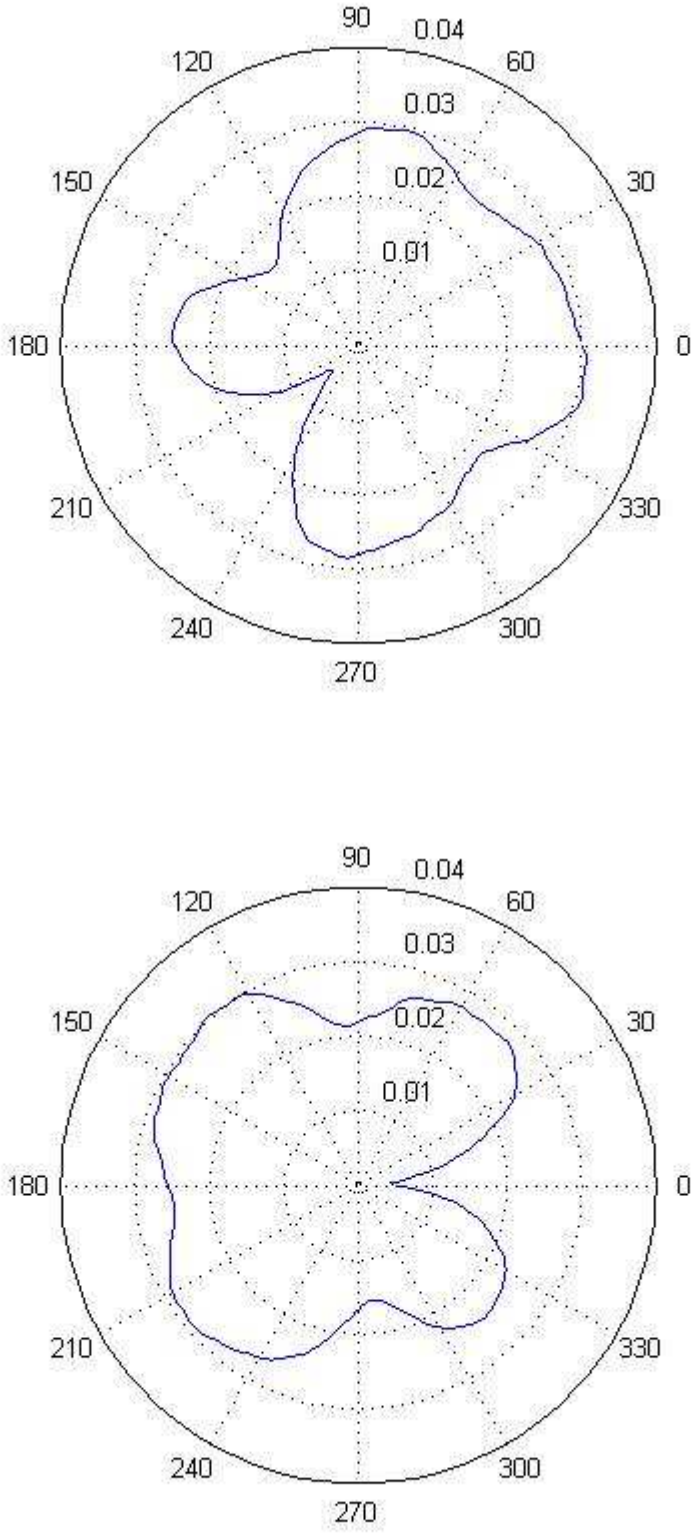

Figure 14: Polar plot of ring 13 belt frame displacement at 2 different times (.08 and .16 sec respectively); results are close to rotations of the mean axle frame shape, although fluctuations are also visible.

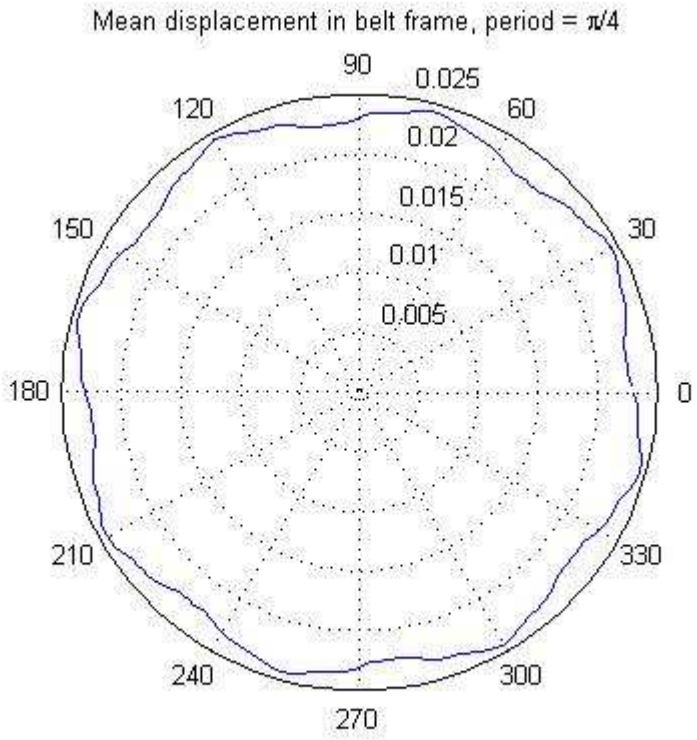

Figure 15: Polar plot of ring 13 mean displacement in the belt frame; result has the expected period of $\pi/4$.

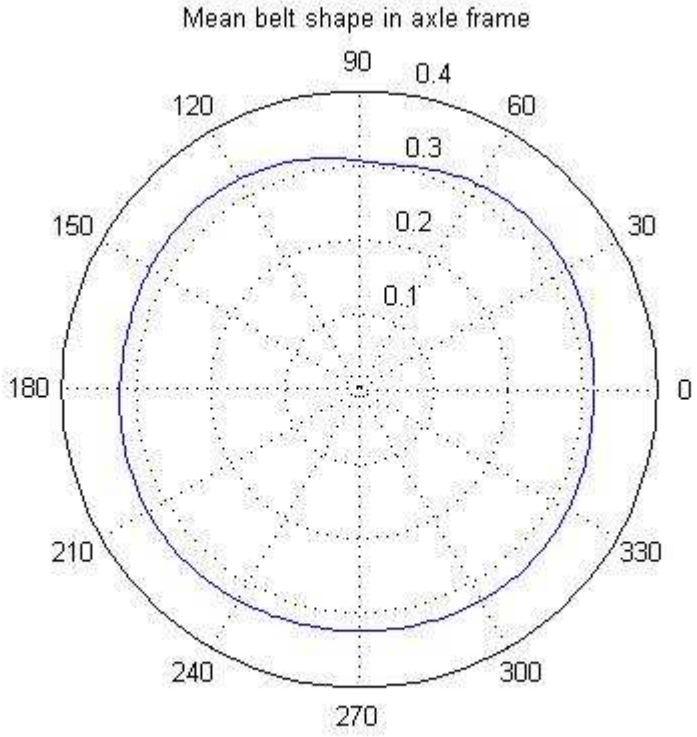

Figure 16: Polar plot of belt shape obtained from lateral averaging.

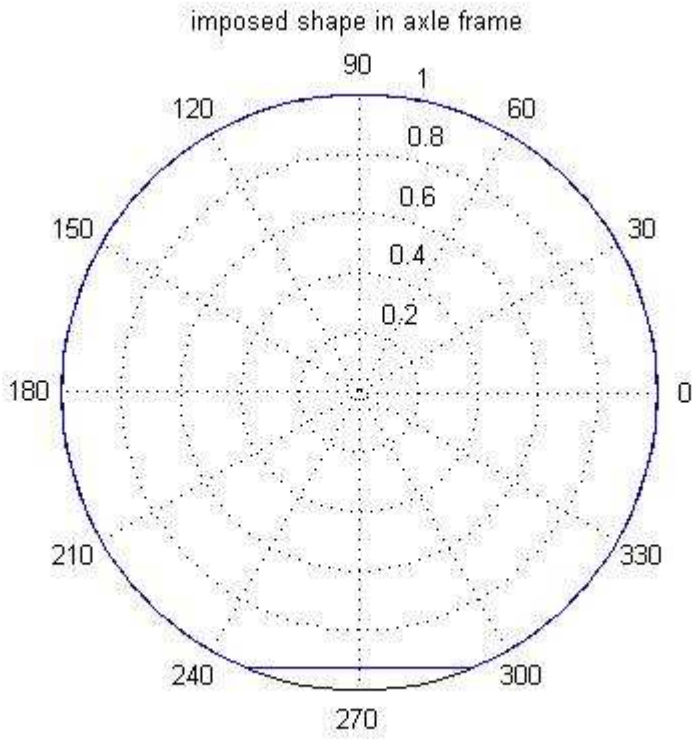

Figure 17: The imposed mean displacement in the axle frame as a function of fixed angle ϕ.

REFERENCES

1. C. Lecomte, W.R. Graham and M. Dale. A shell model for tyre belt vibration. *Journal of Sound and Vibration*, 329 (10), pp1717-1742, 2010.
2. B. Lenoach and W.R. Graham. An integrated tyre vibration model. *Report, Department of Engineering, University of Cambridge*, 2010
3. F. Liu. Tribology of Free-rolling Tyres. *PhD Thesis, University of Cambridge*, 2008.
4. E. Rustighi and S.J. Elliot. Stochastic road excitation and control feasibility in a 2D linear tyre model. *Journal of Sound and Vibration*, 300(3-5), pp490-501, 2007.
5. A. Tsotras and G. Mavros. The simulation of in-plane tyre modal behaviour: a broad modal range comparison between analytical and discretised modelling approaches. *Vehicle System Dynamics,* 47(11), pp1377-1400, 2009.

APPENDIX REMARK ON BELT SHAPE

Ideally, one would like an analytical expression for the displacement in belt frame which would allow an exact reconstruction of the temporal mean in the axle frame. However, we may look at the converse case and see how a given shape, the 'expected' one say, looks in the belt frame. Let us suppose that we are given the mean displacement in the axle frame shown in Figure 17; this may be expressed in the following analytical form

$$\langle v(\phi)\rangle = \begin{cases} \dfrac{\sin\left(\dfrac{3\pi}{2}-\phi_0\right)}{\sin\phi}, & \dfrac{3\pi}{2}-\phi_0 \le \phi \le \dfrac{3\pi}{2}+\phi_0; \\ 1, \quad \text{otherwise} \end{cases} \qquad \text{(A.1)}$$

where the angular brackets denote the average over a period $T = 2\pi/\Omega$

$$\langle F(t)\rangle \equiv \frac{1}{T}\int_0^T F(t)dt$$

It seems reasonable to assume that the full time-dependent displacement in the axle frame may be written as

$$v(t,\phi) = f(\Omega t)\langle v\rangle(\phi)$$

with the average of v as given in equation (A.1). The question is what will the corresponding mean displacement in the rotating frame look like? Define the 'travel times' of the two points marking the ends of the flat section, given by $\phi_{1,2} = \frac{3\pi}{2} \pm \phi_0$ in the axle frame, by $\Omega t_{1,2} = \theta - \phi_{1,2}$. The mean displacement in the belt frame due to the axle frame displacement above is

$$\langle w\rangle(\theta)=\frac{1}{2\pi}\left[\int_0^{\Omega t_1} f(s)ds+\int_{\Omega t_1}^{\Omega t_2}\frac{\sin\left(\frac{3\pi}{2}-\phi_0\right)}{\sin(\theta-s)}f(s)ds+\int_{\Omega t_2}^{2\pi} f(s)ds\right] \quad \text{(A.2)}$$

In the special case where *f* takes a constant value *C*, one obtains

$$\langle w_0\rangle=C\left(1+\frac{2\phi_0}{T}\right)+\frac{C\sin\left(\frac{3\pi}{2}-\phi_0\right)}{2\pi}\left[\log\left(\tan\left(\frac{3\pi}{4}-\frac{\phi_0}{2}\right)\right)-\log\left(\tan\left(\frac{3\pi}{4}+\frac{\phi_0}{2}\right)\right)\right] \quad \text{(A.3)}$$

which is independent of θ.

The latter property is entirely due to *f* being constant; indeed a simple calculation shows that the sum of the first and third terms on the right of equation (A.2) may be written as $g(t_2)-g(t_1)+g(T)$ where $g=\int f(t)dt$. This quantity is independent of θ if, and only if, $g(t_2)-g(t_1)$ depends only on the difference t_2-t_1 which is equivalent to the condition that *f* is constant. Any other choice of *f* produces an angle-dependent mean shape in the rotating frame.

It is interesting to note the equivalent result when *f* fluctuates over a cycle with the same average value *C*, for example if the time-dependent axle frame shape *f (t)* is

$$f(t)=C+\varepsilon\cos(\Omega t)$$

The shape in the belt frame is then

$$\langle w\rangle=\langle w_0\rangle+\frac{\varepsilon\sin\phi_0\sin\theta}{\pi} \quad \text{(A.4)}$$

This illustrates the importance of the fluctuations, as the sole source of shape distortion in the rotating frame, despite their small relative amplitude.